

## Coherent propagation of polaritons in the nonlinear optical regime

S. Schumacher, G. Czycholl, and F. Jahnke

*Institute for Theoretical Physics, University of Bremen, 28334 Bremen, Germany*

(Received 9 September 2005; revised manuscript received 2 December 2005; published 19 January 2006)

The propagation of light pulses through semiconductor heterostructures is studied under the combined influence of polariton effects and optical nonlinearities. For the investigated heterostructures, the light field strongly interacts with the excitonic resonances of the material which leads to a series of polariton resonances. Even in the linear optical regime, the theoretical description is distinctly complicated by the presence of surfaces and interfaces which prevents an analytical solution of the polariton problem. In the coherent nonlinear regime, dynamical changes of the polariton resonances and contributions of biexcitons will be addressed. For this purpose, we combine a microscopic treatment of the boundary problem for the optical interband excitations and the propagating light field in a sample of finite thickness with a description of excitonic and biexcitonic nonlinearities. A practicable scheme is developed to provide a self-consistent solution of generalized Schrödinger and Heitler-London equations for the excitonic and biexcitonic excitations, respectively, together with Maxwell's equations under strict consideration of the boundary conditions. To study the influence of excitonic and biexcitonic nonlinearities on single-pulse propagation, pump and probe transmission experiments, and four-wave mixing spectra, the dependence of the results on the light polarization is analyzed.

DOI: [10.1103/PhysRevB.73.035318](https://doi.org/10.1103/PhysRevB.73.035318)

PACS number(s): 71.36.+c, 71.35.Cc

### I. INTRODUCTION

The resonant interaction of a propagating light field with the excitonic states of a semiconductor heterostructure is a topic of fundamental interest. The strong coupling of the induced material polarization with the optical field leads to polariton resonances, which give rise to polariton beating in time-resolved pulse transmission<sup>1</sup> or provide strong modifications of the excitonic transmission spectra in linear<sup>2-5</sup> or nonlinear<sup>6,7</sup> optical experiments. Polariton effects are directly influenced by the presence of boundaries in the system, which modify the spatial dispersion. Even in the linear optical regime, the proper theoretical description of exciton-polaritons in the presence of system boundaries has been a debated topic for more than 30 years. The physical origin of complications is the coupling of exciton relative and center-of-mass (COM) motion at the sample boundaries. The absence of translation invariance prevents a simple analytical diagonalization of the coupled light and matter Hamiltonian as known from bulk semiconductors.<sup>8</sup> The proper description of the system boundaries for the electromagnetic fields and the excitonic polarization naturally results in a *nonlocal* semiconductor response function as emphasized in Refs. 9–12.

In the frequently used phenomenological approaches<sup>13-15</sup> the coupling of exciton relative and COM motion is neglected which results in a *local* exciton response function where only the COM motion is subject to quantization effects in the confinement geometry; the exciton relative motion is assumed to be independent of the boundaries of the system and is approximated by the result of the infinitely extended medium. To facilitate the solution of the wave equations for the electromagnetic fields within this approach, the introduction of *additional boundary conditions*<sup>13-15</sup> (ABCs) becomes necessary as a result of the above discussed approximations. These ABCs are not uniquely defined and in many situations the specific choice of ABCs can influence

the theoretical predictions.<sup>16</sup> For heterostructures with intermediate thickness, which is large compared to the quantum-well (QW) limit and small enough to prevent the bulk limit, the breakdown of macroscopic polariton models based on ABCs has been demonstrated.<sup>4,5,16</sup> In this case, a microscopic treatment of boundary conditions<sup>16-18</sup> is required to unambiguously describe the corresponding experiments. The QW limit refers to the case where the confinement of carriers yields a quasi-two-dimensional exciton spectrum. Then the optical response at the band edge is dominated by contributions from the lowest subband for electrons and holes, respectively. The QW limit is typically found for layer thicknesses  $\lesssim 2a_0^X$ , with  $a_0^X$  being the bulk exciton Bohr radius. In the opposite limit, for layer thicknesses  $\gtrsim 20a_0^X$ , the bulk limit is obtained, where the confinement is so weak that the hydrogenlike optical response of the bulk material is reproduced as given by the Elliott formula.<sup>8</sup>

Beyond the linear optical regime, optical nonlinearities have been studied in a variety of heterostructures. For polariton effects in optically coupled QWs and microcavities, see Ref. 19. The nonlinear polariton dynamics in these systems has been described both in the coherent and incoherent regime.<sup>20</sup> For a sample thickness approaching the bulk limit, a local approach has been used to model nonlinear pulse propagation effects<sup>21,22</sup> and four-wave mixing signals.<sup>23</sup> Besides the coherent regime, propagation effects have been investigated in the case where incoherent carrier populations play an important role.<sup>6,24</sup>

In this paper we present a consistent theoretical description of nonlinear light propagation for a situation where the spatial extension of the semiconductor is of the order of several Bohr radii. Nonlinear optical transmission spectra are studied in a regime where both the optical fields and the induced material polarization are strongly influenced by the boundaries of the system. In this case a proper microscopic treatment of the boundary conditions becomes, like in the linear regime, indispensable. Our formulation bridges the

gap between the two-dimensional QW limit and the bulklike behavior of the optical response.

For optical excitation with sufficiently weak external fields, the only dynamic quantity which determines the optical properties of the semiconductor material is the excitonic transition amplitude.<sup>8</sup> To extend the theoretical description of propagation effects to the nonlinear regime, the dynamics-controlled truncation<sup>25–27</sup> (DCT) approach is used here to terminate the infinite many-particle hierarchy in the equations of motion for the electronic system. This approach results in a systematic perturbation theory in which all relevant many-particle correlations can, without further approximation, be taken into account in a certain order in the optical field. So far, theories based on this scheme have successfully been applied to quasi-two-dimensional quantum-well systems, e.g., in Refs. 28–33, or to one-dimensional model systems.<sup>34</sup> Our formulation properly accounts for the finite spatial extension of the exciton and biexciton states within a spatially inhomogeneous system. The approach is based on a direct solution of the two-particle and four-particle Schrödinger equations for the exciton and biexciton motion together with Maxwell's equations.<sup>7</sup> We apply microscopic boundary conditions to avoid ambiguities due to ABCs. Excellent agreement of our theoretical results with experimental nonlinear transmission spectra has already been demonstrated for a ZnSe/ZnSSe heterostructure in Ref. 7.

The present paper is organized as follows. The equations of motion for the relevant dynamic quantities, namely the excitonic transition amplitude and the biexcitonic correlation function, are deduced in Sec. II A. To make a solution of the resulting equations of motion possible, a description of the excitonic and biexcitonic problem in the exciton eigenbasis is derived in Sec. II B. Excitonic eigenstates are used here that individually fulfill the physical boundary conditions of the system.<sup>5,18</sup> The required matrix elements are calculated in the new basis. In the quasi-two-dimensional limit, our formulation reduces to the eigenfunction expansion that has successfully been applied to quantum-well systems.<sup>35–37</sup> In contrast to quantum-well models,<sup>32,33,36</sup> however, the expansion of biexciton states in terms of exciton eigenfunctions can here systematically be extended beyond the exciton ground state. In Sec. III A the resulting matrix elements are discussed and the dependence of the biexciton binding energy on the layer thickness is studied. In Sec. III B the theory is applied to the calculation of optical transmission spectra. The complicated interplay of propagation effects and excitonic as well as biexcitonic nonlinearities is discussed in detail. Pronounced signatures of the bound biexciton state and the exciton-exciton scattering continuum are identified. These signatures show a strong dependence on the polarization of the exciting light fields.

## II. THEORY

### A. Equations of motion

Our starting point is the Hamiltonian of the electronic system interacting with an external light field,

$$\mathcal{H} = \mathcal{H}_{\text{kin}} + \mathcal{H}_{\text{dipole}} + \mathcal{H}_{\text{Coulomb}}. \quad (1)$$

It consists of three terms: The kinetic energy of electrons and holes  $\mathcal{H}_{\text{kin}}$ , their dipole coupling to the external light field

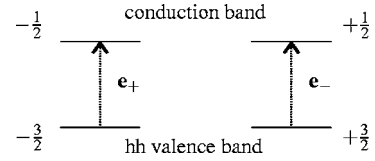


FIG. 1. Schematic illustration of the two-band model with conduction ( $m_j = \pm 1/2$ ) and heavy-hole valence ( $m_j = \pm 3/2$ ) band at the zone center. The optical dipole selection rules are included for light in the circular polarization states  $\mathbf{e}_+$  or  $\mathbf{e}_-$ , respectively.

$\mathcal{H}_{\text{dipole}}$ , and the Coulomb interaction of the carriers  $\mathcal{H}_{\text{Coulomb}}$ .

To simulate a typical experimental setup, we consider a semiconductor layer in a slab geometry<sup>5</sup> with finite thickness in the  $z$  direction and infinite, homogeneous extension in the  $x$ - $y$  plane. A barrier material surrounds the layer of interest to create a heterostructure with spatial confinement potential for electrons and holes in conduction and valence bands, respectively. To describe the spatially inhomogeneous system, it is convenient to define suitable creation  $\psi_{\mathbf{k}}^i(z)$  and annihilation  $\psi_{\mathbf{k}}^i(z)$  operators in the Heisenberg picture, that refer to electrons ( $i=e$ ) with in-plane momentum  $\mathbf{k}=(k_x, k_y)$  or holes ( $i=h$ ) with in-plane momentum  $-\mathbf{k}$  at position  $z$ . To simplify the notation, the time dependence of these operators is not made explicit. The creation and annihilation operators fulfill the fermionic anticommutation relations

$$[\psi_{\mathbf{k}}^i(z), \psi_{\mathbf{k}'}^{j\dagger}(z')]_+ = \delta(z-z')\delta_{\mathbf{k}\mathbf{k}'}\delta_{ij},$$

$$[\psi_{\mathbf{k}}^i(z), \psi_{\mathbf{k}'}^j(z')]_+ = 0, \quad [\psi_{\mathbf{k}}^{i\dagger}(z), \psi_{\mathbf{k}'}^{j\dagger}(z')]_+ = 0. \quad (2)$$

Typically, the crystal structure of the considered semiconductor layer is grown fully strained to the surrounding barrier material, which lifts the degeneracy of valence band states with different magnitude of the  $z$  component of the electronic total angular momentum  $m_j$  at the gamma point. Consequently, in these heterostructures, interband transitions from different valence bands to the conduction band are well separated and can be excited selectively in the optical spectra.<sup>5,16</sup> In order not to overburden our theory and to concentrate on more important details, in the following, the formulation is restricted to a two-band model with spin degenerate heavy-hole valence and conduction band as illustrated in Fig. 1. For this system, the  $z$  component of the total angular momentum  $m_j$  can take the values  $\pm 1/2$  for electrons and  $\pm 3/2$  for holes which are in the following included in the band indices  $e, h$  to simplify the notation.

Using the above definitions the kinetic part of the Hamiltonian (1) takes the form

$$\mathcal{H}_{\text{kin}} = \sum_{\mathbf{k}} \int dz \left[ \sum_e \psi_{\mathbf{k}}^{e\dagger}(z) \varepsilon_{\mathbf{k},z}^e \psi_{\mathbf{k}}^e(z) + \sum_h \psi_{\mathbf{k}}^{h\dagger}(z) \varepsilon_{\mathbf{k},z}^h \psi_{\mathbf{k}}^h(z) \right], \quad (3)$$

with the one-particle energy operators

$$\varepsilon_{\mathbf{k},z}^i = \frac{\hbar^2 \mathbf{k}^2}{2m_i^*} - \frac{\hbar^2}{2m_i^*} \frac{\partial^2}{\partial z_i^2} + E_{\text{gap}} \delta_{ie} + V_{\text{ext}}^i(z_i) \quad (4)$$

for electrons ( $i=e$ ) and holes ( $i=h$ ) in effective mass approximation;  $m_e^*$  and  $m_h^*$  denote the effective electron and hole masses, respectively. The external potential  $V_{\text{ext}}^i(z)$  is used to model the band offsets in the heterostructure. The interband dipole interaction of the electronic system with the external electromagnetic field is given by

$$\mathcal{H}_{\text{dipole}} = - \sum_{\mathbf{k} \in \text{eh}} \int dz [\psi_{\mathbf{k}}^{e\dagger}(z) \psi_{\mathbf{k}}^{h\dagger}(z) \mathbf{d}_{\text{eh}} \mathbf{E}(z) + \psi_{\mathbf{k}}^h(z) \psi_{\mathbf{k}}^e(z) \mathbf{d}_{\text{eh}}^* \mathbf{E}(z)], \quad (5)$$

with the dipole matrix element  $\mathbf{d}_{\text{eh}}(\mathbf{k}, z_e - z_h) = \mathbf{d}_{\text{eh}} \delta(z_e - z_h)$ , which is assumed to be local in real space and  $\mathbf{k}$  independent.

The Coulomb interaction of electrons and holes in envelope approximation has the form

$$\begin{aligned} \mathcal{H}_{\text{Coulomb}} = & \frac{1}{2} \sum_{\mathbf{k}\mathbf{k}'\mathbf{q}} \int dz dz' V_{\mathbf{q}}^{zz'} \\ & \times \left[ \sum_{ee'} \psi_{\mathbf{k}+\mathbf{q}}^{e\dagger}(z) \psi_{\mathbf{k}'-\mathbf{q}}^{e'\dagger}(z') \psi_{\mathbf{k}'}^{e'}(z') \psi_{\mathbf{k}}^e(z) \right. \\ & + \sum_{hh'} \psi_{\mathbf{k}+\mathbf{q}}^{h\dagger}(z) \psi_{\mathbf{k}'-\mathbf{q}}^{h'\dagger}(z') \psi_{\mathbf{k}'}^{h'}(z') \psi_{\mathbf{k}}^h(z) \\ & \left. - 2 \sum_{eh} \psi_{\mathbf{k}+\mathbf{q}}^{e\dagger}(z) \psi_{\mathbf{k}'-\mathbf{q}}^{h'\dagger}(z') \psi_{\mathbf{k}'}^{h'}(z') \psi_{\mathbf{k}}^e(z) \right], \quad (6) \end{aligned}$$

with the Coulomb matrix elements

$$V_{\mathbf{q}}^{zz'} = \frac{e^2}{2\varepsilon_0 n_{\text{bg}}^2} \frac{\exp(-|\mathbf{q}||z-z'|)}{|\mathbf{q}|}. \quad (7)$$

Here  $e$  is the magnitude of the electronic charge,  $\varepsilon_0$  is the vacuum dielectric constant, and  $n_{\text{bg}}$  is the nonresonant background refractive index of the semiconductor material.

To describe the interaction of the electronic system with an external electromagnetic field on a microscopic level, the

resonant contribution to the macroscopic polarization,

$$\mathbf{P}(z,t) = \sum_{\text{ehk}} \mathbf{d}_{\text{eh}}^* p_{(\mathbf{k},z,z)}^{\text{eh}}(t) = \sum_{\text{ehk}} \mathbf{e}_{\text{eh}} d_{\text{eh}}^* p_{(\mathbf{k},z,z)}^{\text{eh}}(t), \quad (8)$$

is calculated in terms of the excitonic transition amplitude,

$$p_{(\mathbf{k},z,z')}^{\text{eh}}(t) = \langle \psi_{\mathbf{k}}^h(z') \psi_{\mathbf{k}}^e(z) \rangle. \quad (9)$$

The dipole selection rules, visualized in Fig. 1, and the optical polarization state of the macroscopic polarization (8) can be represented using

$$\mathbf{d}_{-\frac{1}{2}-\frac{3}{2}} = d_{\text{eh}} \mathbf{e}_+ \quad \text{and} \quad \mathbf{d}_{+\frac{1}{2}+\frac{3}{2}} = d_{\text{eh}} \mathbf{e}_-, \quad (10)$$

with  $\mathbf{e}_{\pm} = 1/\sqrt{2}(\mathbf{e}_x \pm i\mathbf{e}_y)$  and the Cartesian basis vectors  $\mathbf{e}_x$  and  $\mathbf{e}_y$ . The macroscopic polarization, expressed in terms of the two circularly polarized contributions, is given by

$$\mathbf{P}(z,t) = P_+(z,t) \mathbf{e}_+ + P_-(z,t) \mathbf{e}_- = d_{\text{eh}}^* \sum_{\mathbf{k}} \left( p_{(\mathbf{k},z,z)}^{-\frac{1}{2}-\frac{3}{2}} \mathbf{e}_+ + p_{(\mathbf{k},z,z)}^{+\frac{1}{2}+\frac{3}{2}} \mathbf{e}_- \right). \quad (11)$$

With the ansatz  $\mathbf{E}(\mathbf{r},t) = E_+(z,t) \mathbf{e}_+ + E_-(z,t) \mathbf{e}_-$  and  $\mathbf{B}(\mathbf{r},t) = B_+(z,t) \mathbf{ie}_+ + B_-(z,t) \mathbf{ie}_-$  for circularly polarized transverse electromagnetic fields, Maxwell's equations are decoupled for each circular polarization state. For propagation in the  $z$  direction they can be used in the one-dimensional form

$$n_{\text{bg}}^2 \frac{\partial}{\partial t} E_{\pm}(z,t) = -c_0^2 \frac{\partial}{\partial z} B_{\pm}(z,t) - \frac{1}{\varepsilon_0} \frac{\partial}{\partial t} P_{\pm}(z,t), \quad (12)$$

$$\frac{\partial}{\partial t} B_{\pm}(z,t) = -\frac{\partial}{\partial z} E_{\pm}(z,t). \quad (13)$$

The dynamics of the excitonic transition amplitude (9) follows from Heisenberg's equation of motion for the operators  $\psi_{\mathbf{k}}^e(z)$ ,  $\psi_{\mathbf{k}}^h(z)$  with the Hamiltonian (1) and the commutation relations (2). Within the DCT formalism,<sup>25-27</sup> the macroscopic polarization of the system is calculated up to third order in the electromagnetic field. This yields the following equations for the dynamics of the excitonic transition amplitude<sup>38</sup>

$$\begin{aligned} i\hbar \frac{\partial}{\partial t} p_{(\mathbf{k},z_e,z_h)}^{\text{eh}} = & (\varepsilon_{\mathbf{k},z_e}^e + \varepsilon_{\mathbf{k},z_h}^h) p_{(\mathbf{k},z_e,z_h)}^{\text{eh}} - \sum_{\mathbf{k}'} V_{\mathbf{k}-\mathbf{k}'}^{z_e z_h} p_{(\mathbf{k}',z_e,z_h)}^{\text{eh}} - \mathbf{d}_{\text{eh}} \mathbf{E}(z_e) \delta(z_e - z_h) + \sum_{e'h'} \left[ \mathbf{d}_{\text{eh}'} \mathbf{E}(z_e) \int dz p_{(\mathbf{k},z,z_e)}^{*e'h'} p_{(\mathbf{k},z,z_h)}^{e'h} \right. \\ & + \mathbf{d}_{e'h} \mathbf{E}(z_h) \int dz p_{(\mathbf{k},z_h,z)}^{*e'h'} p_{(\mathbf{k},z_e,z)}^{\text{eh}'} \left. \right] + \sum_{\mathbf{k}'e'h'} \int dz_e' dz_h' \left[ \left( V_{\mathbf{k}-\mathbf{k}'}^{z_e' z_h} p_{(\mathbf{k},z_e',z_h')}^{*e'h'} - V_{\mathbf{k}-\mathbf{k}'}^{z_h' z_e} p_{(\mathbf{k}',z_e',z_h')}^{*e'h'} \right) p_{(\mathbf{k},z_e,z_h)}^{\text{eh}'} p_{(\mathbf{k}',z_e',z_h')}^{e'h} \right. \\ & + \left( V_{\mathbf{k}-\mathbf{k}'}^{z_h' z_e} p_{(\mathbf{k},z_e',z_h')}^{*e'h'} - V_{\mathbf{k}-\mathbf{k}'}^{z_e' z_h} p_{(\mathbf{k}',z_e',z_h')}^{*e'h'} \right) p_{(\mathbf{k}',z_e,z_h)}^{\text{eh}'} p_{(\mathbf{k},z_e',z_h')}^{e'h} \left. \right] + \sum_{\mathbf{k}'qe'h'} \int dz_e' dz_h' \left[ \left( V_{\mathbf{q}}^{z_h' z_h} p_{(\mathbf{k}'+\mathbf{q},z_e',z_h')}^{*e'h'} \right. \right. \\ & \left. \left. - V_{\mathbf{q}}^{z_e' z_h} p_{(\mathbf{k}',z_e',z_h')}^{*e'h'} \right) b_{\text{eh}}^{e'h'}(\mathbf{k}'+\mathbf{q},z_e',\mathbf{k}',z_h') + \left( V_{\mathbf{q}}^{z_e' z_e} p_{(\mathbf{k}'+\mathbf{q},z_e',z_h')}^{*e'h'} - V_{\mathbf{q}}^{z_h' z_e} p_{(\mathbf{k}',z_e',z_h')}^{*e'h'} \right) b_{\text{eh}}^{e'h'}(\mathbf{k}+\mathbf{q},z_e,\mathbf{k},z_h) \right]. \quad (14) \end{aligned}$$

In Eq. (14) the biexcitonic correlation function

$$b_{eh}^{e'h'}(\mathbf{k}_2, z_2, \mathbf{k}_1, z_1) = \langle \psi_{\mathbf{k}_1}^{h'}(z_1) \psi_{\mathbf{k}_2}^{e'}(z_2) \psi_{\mathbf{k}_3}^h(z_3) \psi_{\mathbf{k}_4}^e(z_4) \rangle - \langle \psi_{\mathbf{k}_1}^{h'}(z_1) \psi_{\mathbf{k}_2}^{e'}(z_2) \rangle \langle \psi_{\mathbf{k}_3}^h(z_3) \psi_{\mathbf{k}_4}^e(z_4) \rangle + \langle \psi_{\mathbf{k}_1}^{h'}(z_1) \psi_{\mathbf{k}_4}^e(z_4) \rangle \langle \psi_{\mathbf{k}_3}^h(z_3) \psi_{\mathbf{k}_2}^{e'}(z_2) \rangle, \quad (15)$$

has been introduced, following Ref. 39. This definition is advantageous since it leads to the explicit appearance of the Hartree-Fock contributions to the third order coherent nonlinearities in Eq. (14) via lines 2–4. The coupling to the biexcitonic correlation function, lines 5, 6 in Eq. (14), determines the third order contributions beyond Hartree-Fock. Therefore, the definition in Eq. (15) allows for an identification of effective two-particle (Hartree-Fock) and four-particle (biexcitonic) third order contributions to the coherent dynamics of the material polarization. For the factorization of the relevant density matrix elements in the coherent limit, see Appendix A.

The equation of motion for the biexcitonic correlation function (15), introduced in Eq. (14), reads

$$\begin{aligned} i\hbar \frac{\partial}{\partial t} b_{eh}^{e'h'}(\mathbf{k}+\mathbf{q}, z_e, \mathbf{k}, z_h) &= \left( \mathcal{E}_{\mathbf{k}+\mathbf{q}, z_e}^e + \mathcal{E}_{\mathbf{k}, z_h}^h + \mathcal{E}_{\mathbf{k}', z_e'}^{e'} + \mathcal{E}_{\mathbf{k}'+\mathbf{q}, z_h'}^{h'} \right) b_{eh}^{e'h'}(\mathbf{k}', z_e', \mathbf{k}'+\mathbf{q}, z_h') + \sum_{\mathbf{q}'} \left[ V_{\mathbf{q}'}^{z_h' z_h} b_{eh}^{e'h'}(\mathbf{k}', z_e', \mathbf{k}'+\mathbf{q}+\mathbf{q}', z_h') \right. \\ &+ V_{\mathbf{q}'}^{z_e' z_e} b_{eh}^{e'h'}(\mathbf{k}'-\mathbf{q}', z_e', \mathbf{k}'+\mathbf{q}, z_h') - V_{\mathbf{q}'}^{z_h' z_e'} b_{eh}^{e'h'}(\mathbf{k}'+\mathbf{q}', z_e', \mathbf{k}'+\mathbf{q}+\mathbf{q}', z_h') - V_{\mathbf{q}'}^{z_e' z_h} b_{eh}^{e'h'}(\mathbf{k}'+\mathbf{q}', z_e', \mathbf{k}'+\mathbf{q}, z_h') \\ &- V_{\mathbf{q}'}^{z_h z_e} b_{eh}^{e'h'}(\mathbf{k}'+\mathbf{q}', z_e, \mathbf{k}'+\mathbf{q}, z_h) - V_{\mathbf{q}'}^{z_h z_e'} b_{eh}^{e'h'}(\mathbf{k}', z_e', \mathbf{k}'+\mathbf{q}+\mathbf{q}', z_h') \left. \right] + \left( V_{\mathbf{q}}^{z_h z_h} P(\mathbf{k}', z_e', z_h') \right. \\ &- V_{\mathbf{q}}^{z_e z_e} P(\mathbf{k}'+\mathbf{q}, z_e, z_h) \left. \right) P(\mathbf{k}+\mathbf{q}, z_e, z_h) + \left( V_{\mathbf{q}}^{z_e z_e} P(\mathbf{k}'+\mathbf{q}, z_e', z_h') - V_{\mathbf{q}}^{z_h z_h} P(\mathbf{k}', z_e', z_h') \right) P(\mathbf{k}, z_e, z_h) - \left( V_{\mathbf{k}-\mathbf{k}'}^{z_h z_h} P(\mathbf{k}', z_e', z_h') \right. \\ &- V_{\mathbf{k}-\mathbf{k}'}^{z_e z_e} P(\mathbf{k}, z_e, z_h) \left. \right) P(\mathbf{k}+\mathbf{q}, z_e, z_h) - \left( V_{\mathbf{k}-\mathbf{k}'}^{z_e z_e} P(\mathbf{k}, z_e, z_h) - V_{\mathbf{k}-\mathbf{k}'}^{z_h z_h} P(\mathbf{k}', z_e', z_h') \right) P(\mathbf{k}'+\mathbf{q}, z_e, z_h). \quad (16) \end{aligned}$$

The discussed coupled set of equations of motion for the excitonic polarization (14) and the biexcitonic correlation function (16) represents a generalization of the result for the quasi-two-dimensional quantum-well system. It additionally includes the nonlocal space dependence of excitonic and biexcitonic excitations<sup>36,39</sup> for a layer with finite thickness and allows the application of microscopic boundary conditions. Equations (14) and (16) together with Maxwell's equations (12) and (13) for the electromagnetic field represent a microscopic theory for nonlinear polariton propagation in the coherent limit. Both propagation effects and all third order coherent optical nonlinearities, which are Hartree-Fock contributions and biexcitonic correlations, are included.

Even the direct solution of Eq. (14) for the excitonic transition amplitude in the simpler form without optical nonlinearities turns out to be numerically very demanding,<sup>16</sup> The direct solution of Eqs. (14) and (16), including the full biexcitonic problem, is numerically far beyond practical possibilities. However, a solution of the coupled exciton-biexciton-light dynamics can be achieved by a transition to the exciton eigenbasis. The expansions for the excitonic transition amplitude and the biexcitonic correlation function in terms of exciton eigenstates of the *finite-thickness layer* and the resulting equations of motion for the time dependent expansion coefficients are formulated in the next section.

### B. The exciton eigenbasis

The expansion of the excitonic transition amplitude in terms of exciton eigenstates  $\phi_m(\mathbf{k}, z_e, z_h)$  yields

$$p_{(k, z_e, z_h)}^{eh}(t) = \sum_m p_m^{eh}(t) \phi_m(\mathbf{k}, z_e, z_h). \quad (17)$$

In our approach the exciton eigenstates  $\phi_m(\mathbf{k}, z_e, z_h)$  are directly determined for the confinement geometry, so that each

eigenstate individually fulfills the physical boundary conditions of the system.<sup>5,18</sup> The time-dependent expansion coefficients  $p_m^{eh}(t)$  are connected to the corresponding interband transitions in the two-band model. The electron-hole one-particle energies and the Coulomb interaction in (1) do not depend on the  $z$  component of electron and hole angular momenta, which are included in our notation in the band index  $e, h$ . Therefore, spin-independent exciton eigenstates  $\phi_m(\mathbf{k}, z_e, z_h)$  enter the expansion (17).

Following the ansatz in Ref. 39, using symmetric and antisymmetric linear combinations of two-exciton product states, appropriate for the symmetry of the four-fermion states, the expansion of the electronic singlet ( $\lambda=-1$ ) and triplet ( $\lambda=+1$ ) configurations of the biexcitonic correlation function takes the form<sup>40</sup>

$$\begin{aligned} b_{eh}^{e'h\lambda}(\mathbf{k}_2, z_2, \mathbf{k}_1, z_1) &= \sum_{nm} [\phi_n(\alpha \mathbf{k}_4 + \beta \mathbf{k}_3, z_4, z_3) \phi_m(\alpha \mathbf{k}_2 \\ &+ \beta \mathbf{k}_1, z_2, z_1) \times b_{nm}^{eh e'h\lambda}(\mathbf{k}_4 - \mathbf{k}_3, t) \\ &- \lambda \phi_n(\alpha \mathbf{k}_2 + \beta \mathbf{k}_3, z_2, z_3) \phi_m(\alpha \mathbf{k}_4 \\ &+ \beta \mathbf{k}_1, z_4, z_1) \times b_{nm}^{eh e'h\lambda}(\mathbf{k}_2 - \mathbf{k}_3, t)], \quad (18) \end{aligned}$$

with

$$b_{eh}^{e'h'}(\mathbf{k}_2, z_2, \mathbf{k}_1, z_1) = b_{eh}^{e'h'+(\mathbf{k}_2, z_2, \mathbf{k}_1, z_1)} + b_{eh}^{e'h'-(\mathbf{k}_2, z_2, \mathbf{k}_1, z_1)}.$$

Here  $\alpha = m_h^*/M^*$  and  $\beta = m_e^*/M^*$  are the ratio of the hole and the electron masses to the total exciton mass  $M^* = m_e^* + m_h^*$ . To account for a nonvanishing in-plane center-of-mass momentum for the exciton states, which is induced by the exciton-exciton Coulomb interaction, the expansion coefficients

$b_{nm}^{\text{eh}^{\prime}\text{h}^{\prime}\lambda}(\mathbf{q})$  depend on the internal excitonic quantum numbers  $n, m$  and on the two-exciton relative momentum  $\mathbf{q}$ . With the expansion (18) for the biexcitonic correlation function, proper antisymmetry with respect to particle interchange is guaranteed for each term with fixed quantum numbers  $n, m$ . This is of particular importance for the evaluations in a truncated exciton basis.<sup>39</sup> Inserting the expansions (17) and (18) into Eqs. (14) and (16), a somewhat lengthy but straight forward calculation yields the closed set of equations of motion for the coefficients of the excitonic transition amplitude

$$\begin{aligned}
i\hbar \frac{d}{dt} p_m^{\text{eh}} &= \varepsilon_m p_m^{\text{eh}} - \mathbf{d}_{\text{eh}} \int dz \mathbf{E}(z) \sum_{\mathbf{k}} \phi_m^*(\mathbf{k}, z, z) \\
&+ \sum_{m'ne'h'} p_{m'}^{*e'h'} \left[ p_n^{e'h} \int dz_e \mathbf{d}_{\text{eh}} \mathbf{E}(z_e) R_{mm'n}^1(z_e) \right. \\
&+ \left. p_n^{\text{eh}'} \int dz_h \mathbf{d}_{e'h} \mathbf{E}(z_h) R_{mm'n}^2(z_h) \right] \\
&+ \sum_{m'nm'e'h'} p_{m'}^{*e'h'} p_n^{\text{eh}'} p_{n'}^{e'h} V_{mm'nn'}^{\text{HF}} \\
&+ \sum_{ne'h'} p_n^{*e'h'} \sum_{\mathbf{q}'m'\lambda} W_{n'm'mn}^{\text{XX}\lambda*}(\mathbf{q}, 0) b_{n'm'}^{\text{eh}^{\prime}\text{h}^{\prime}\lambda}(\mathbf{q}),
\end{aligned} \tag{19}$$

and for the biexcitonic correlation function

$$\begin{aligned}
i\hbar \frac{d}{dt} b_{nm}^{\text{eh}^{\prime}\text{h}^{\prime}\lambda}(\mathbf{q}) &= \sum_{n'm'\mathbf{q}'} H_{nmm'm'}^{\text{XX}\lambda}(\mathbf{q}, \mathbf{q}') b_{n'm'}^{\text{eh}^{\prime}\text{h}^{\prime}\lambda}(\mathbf{q}') \\
&+ \frac{1}{2} \sum_{n'm'rs\mathbf{q}'} \{ (1 - \lambda S)_{nmrs}^{-1}(\mathbf{q}, \mathbf{q}') \\
&\times W_{rsn'm'}^{\text{XX}\lambda}(\mathbf{q}', 0) [p_n^{\text{eh}} p_{m'}^{e'h'} + \lambda p_{n'}^{e'h} p_{m'}^{\text{eh}'}] \}.
\end{aligned} \tag{20}$$

The required matrix elements are given and discussed in Appendix B. They contain the nonlocal space dependence of the exciton and biexciton states in the spatially inhomogeneous system. Details concerning the numerical evaluation of these matrix elements are summarized in Appendix C. The biexcitonic Hamiltonian matrix  $H_{nmm'm'}^{\text{XX}\lambda}(\mathbf{q}, \mathbf{q}')$  determines the spectral properties of the two-electron-two-hole states in the system; it contains the bound biexciton state as well as the exciton-exciton scattering continuum.

So far, calculations in the excitonic eigenbasis have been successfully applied to quasi-two-dimensional quantum-well systems, where experimental findings could be reproduced and analyzed for different excitation conditions.<sup>32,33</sup> In a typical experimental situation, where the electronic system is optically excited by a laser pulse with central frequency tuned to or below the fundamental exciton resonance, only a selected part of the excitonic spectrum provides the dominant contribution to the nonlinear response of the system. Due to the large energy separation of the excitonic ground state from the neglected part of the spectrum, for these systems it is a meaningful approximation only to take into ac-

count the dominant  $1s$  contribution. This way the main features of biexcitonic correlations around the fundamental exciton resonance<sup>41</sup> can be included. In this approximation, the optical properties of the system can be well described with a finite number of exciton eigenstates in the expansions (17) and (18), even for a semiconductor layer with finite thickness in the  $z$  direction.<sup>5,7</sup>

In the considered slab geometry, the low energy part of the exciton spectrum consists of a finite number of spectrally separated exciton states with in-plane rotation invariance ( $s$  symmetry) and different spatial structures in the  $z$  direction. In principle, on the level of two-electron-two-hole correlations (biexcitons), exciton-exciton Coulomb interaction yields a coupling to energetically higher exciton states, including exciton states having non in-plane  $s$  symmetry. Exciton states, which are energetically outside the considered spectral range for the optical excitations are neglected in this work, including higher states with  $s$  symmetry as well as states with non- $s$  symmetry. In principle, the Coulomb coupling to these higher exciton states may influence the biexcitonic spectral properties even in the considered low energy part of the spectrum. An increase of the biexciton binding energy and additional contributions to the biexciton continuum can be expected. Nevertheless, our results clearly demonstrate that the dominant contributions to the nonlinear optical response can already be obtained even with a truncated exciton basis, where only the lowest exciton states with  $s$  symmetry are included.<sup>7</sup> The higher exciton states with  $s$  and with non- $s$  symmetry will be more important if more than the low energy part of the spectrum is investigated and optically excited. In that case, contributions from higher exciton states are expected to become even qualitatively important.

For the numerical evaluation, we use the following in-plane angular momentum decomposition of the biexcitonic correlation function and the matrix elements in the two-exciton product basis, following Ref. 36:

$$b_{nm}^{\text{eh}^{\prime}\text{h}^{\prime}\lambda}(\mathbf{q}) = \sum_{\mu} e^{i\mu\phi_q} b_{nm}^{\text{eh}^{\prime}\text{h}^{\prime}\lambda\mu}(q), \tag{21}$$

$$M_{nmm'm'}^{\mu\mu'}(\mathbf{q}, \mathbf{q}') = \sum_{\mu\mu'} e^{i\mu\phi_q} M_{nmm'm'}^{\mu\mu'}(q, q') e^{-i\mu'\phi_{q'}}. \tag{22}$$

Here  $M_{nmm'm'}^{\mu\mu'}(\mathbf{q}, \mathbf{q}')$  represents one of the matrix elements in the two-exciton product basis needed in the equations of motion (19) and (20). The exciton eigenfunctions  $\phi_m(\mathbf{k}, z_e, z_h)$  are eigenfunctions to the in-plane angular momentum operator with quantum numbers  $\mu_n$  and  $\mu_m$  for the two contributing excitons in states  $n, m$ . Taking into account the angular momentum  $\mu$  for the two-exciton relative motion, the total in-plane angular momentum of the two-exciton system is  $\mu_{\text{tot}} = \mu + \mu_n + \mu_m$ . Due to the rotation invariance of the semiconductor heterostructure along the  $z$  axis, the in-plane total angular momentum  $\mu_{\text{tot}}$  of the two-exciton system is conserved. Consequently, the Fourier coefficients  $M_{nmm'm'}^{\mu\mu'}(q, q')$  in Eq. (22) are block diagonal for fixed  $\mu_{\text{tot}}$ . The Coulomb coupling of exciton states with different in-plane symmetry is neglected according to the above discussion. Then usage

of the expansions (21) and (22) with the equation of motion (20) yields decoupled sets of equations for the expansion coefficients  $b_{nm}^{\text{eh}'\lambda\mu}(q)$  for fixed  $\mu$ . Due to the system symmetry, including the in-plane homogeneity of the exciting optical fields, the in-plane total angular momentum  $\mu_{\text{tot}}$  vanishes for each biexciton. Hence, the only relevant matrix elements in the two-exciton product basis are given by

$$\begin{aligned} M_{nmn'm'}(q, q') &= M_{nmn'm'}^{00}(q, q') \\ &= \int_0^{2\pi} \frac{d\phi_{q'}}{2\pi} M_{nmn'm'}(q, 0, q', \phi_{q'}) \end{aligned} \quad (23)$$

and only the  $b_{nm}^{\text{eh}'\lambda}(q) = b_{nm}^{\text{eh}'\lambda\mu=0}(q)$  contribution to the biexcitonic correlation function (21) is driven. Therefore, restricting the expansions (17) and (18) to in-plane s-shaped exciton states and using all matrix elements in their angular averaged version (23), the projection of the equations of motion (19) and (20) to the in-plane  $s$  subspace of exciton states is obtained.

### III. RESULTS AND DISCUSSION

In Sec. III A the biexcitonic spectral properties and the Coulomb matrix elements in the antisymmetrized two-exciton product basis are discussed. In Sec. III B results for nonlinear transmission spectra of a single light pulse as well as for typical pump and probe and four-wave mixing geometries are presented. The theoretical analysis of the fundamental physics in our model in this section is done for a GaAs layer, surrounded by infinitely high potential barriers in the  $z$  direction. This system is chosen here, in order to keep the discussion of the theoretical results as simple and expressive as possible. The application of our theory to a ZnSe/ZnSSe heterostructure with finite-height confinement potentials has successfully been demonstrated in Ref. 7 in a direct theory-experiment comparison.

#### A. Coulomb matrix elements and the biexciton binding energy

The main purpose of our approach is to describe the fundamental excitonic and biexcitonic many-particle effects that contribute to the coherent optical response of the system. Regarding the calculated values of the biexciton binding energy, one has to keep in mind that the above discussed approximations are expected to somewhat underestimate the result. While there are more accurate methods to calculate the biexciton binding energy itself, we give the results of our approach for completeness but concentrate on coherent biexcitonic optical nonlinearities.

The exciton states in the confinement geometry are labeled by consecutive numbers, starting with the ground state. The matrix elements in the two-exciton product basis are given in Appendix B. For a fixed set of internal excitonic quantum numbers  $n, m, n', m'$  in the two-exciton product basis, the direct and exchange Coulomb matrix elements (B1) and (B2) can be classified by on-site ( $n=m=n'=m'$ ), intersite diagonal ( $n=n'$  and  $m=m'$  and  $n \neq m$ ) and off-diagonal ( $n \neq n'$  or  $m \neq m'$ ) blocks, respectively. Note that the names

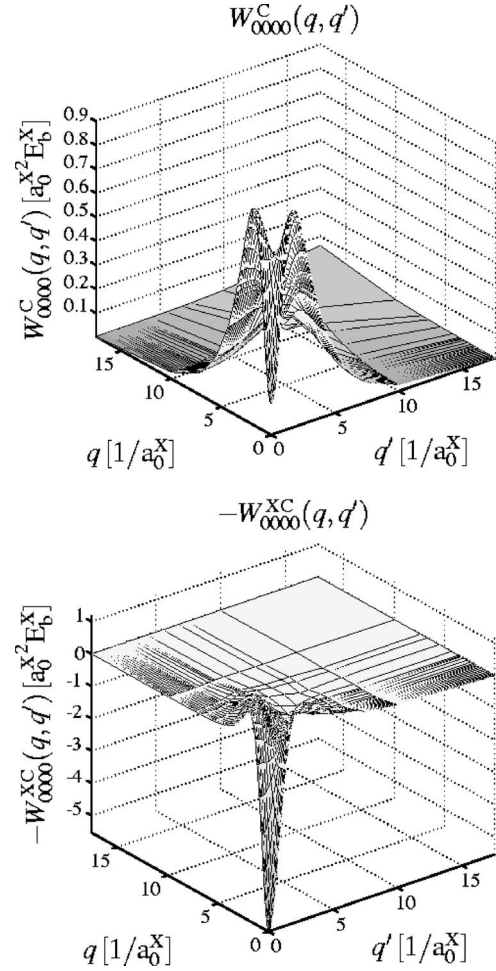


FIG. 2. Examples for on-site Coulomb matrix elements. Direct (top) and exchange (bottom) exciton-exciton interaction.

“on-site” and “intersite” should not be taken literally here since they are just used to provide a convenient classification of the different combinations of excitonic quantum numbers in our system by a short name; it must not be misinterpreted as a distinction between “lattice sites” as known from tight-binding or Hubbard models. For better comparison, energies are normalized to the bulk exciton binding energy  $E_b^X(3D)$  and lengths to the bulk exciton Bohr radius  $a_0^X$ .

The results are discussed for typical GaAs parameters,  $m_e^* = 0.067 m_0$ ,  $m_h^* = 0.457 m_0$ , where  $m_0$  denotes the bare electron mass, and  $n_{\text{bg}} = 3.71$  is the background refractive index.

Figures 2–4 show elements of the direct  $W_{nmn'm'}^C(q, q')$  and exchange  $W_{nmn'm'}^{XC}(q, q')$  Coulomb matrices in the two-exciton product basis for a layer thickness of five exciton Bohr radii. Depending on the internal exciton quantum numbers  $n, m, n', m'$  the direct matrix elements show qualitatively different shapes. Examples are depicted in the upper parts of Figs. 2–4. For the spatially inhomogeneous system the direct Coulomb matrix elements do not vanish in the  $q \rightarrow 0, q' \rightarrow 0$  limit, even not for the on-site matrix element  $W_{0000}^C(q, q')$ , shown in Fig. 2. This is due to the finite layer thickness in our system which leads to contributions from several subbands in contradiction to the results in Ref. 36 for

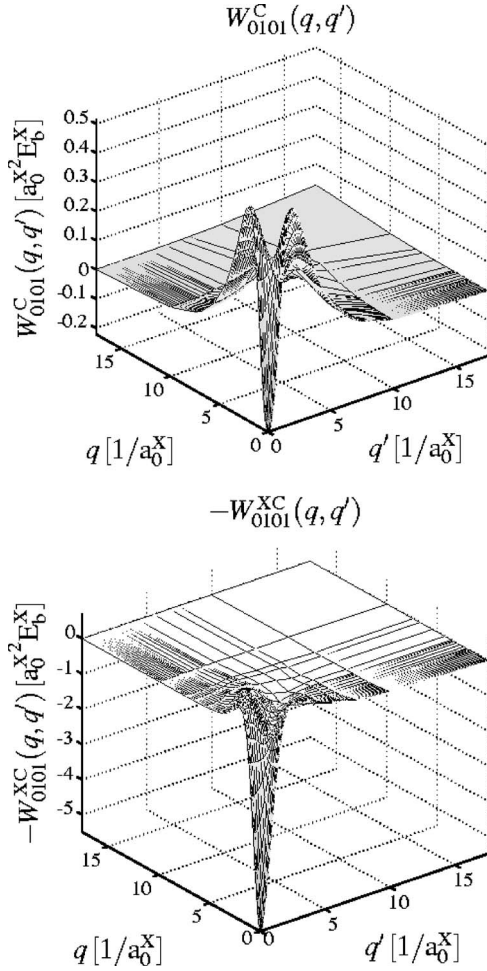


FIG. 3. Examples for intersite diagonal Coulomb matrix elements. Direct (top) and exchange (bottom) exciton-exciton interaction.

the two-dimensional quantum-well system. Figure 3 shows an intersite block of the direct Coulomb matrix. Figure 4 gives an example for an off-diagonal block. The two-exciton exchange matrix elements  $W_{nmn'm'}^{XC}(q, q')$  show a similar shape for all on-site and intersite matrix elements, only quantitative differences are obtained, see Figs. 2 and 3 for two examples. Contributions for wave vectors with magnitude  $q$  and  $q'$  larger than  $20/a_0^X$  can be neglected since all Coulomb matrix elements vanish for large  $q$  and  $q'$ .

The dependence of the exciton (x) and the biexciton (o) binding energy on the layer thickness  $L$  is shown in Fig. 5. Within our model, the biexciton binding energy  $E_b^{XX}(L)$  depends on the number of exciton states that are included to build the biexciton Hamiltonian matrix  $H_{nmn'm'}^{XXX}(\mathbf{q}, \mathbf{q}')$ . The number of exciton states in the considered spectral range in the calculations varies with the layer thickness. It is determined by the level spacing of the lowest exciton states which is strongly influenced by the spatial confinement in the  $z$  direction. We have one state with  $1s$  in-plane symmetry for a layer thickness of  $1a_0^X$  and  $2a_0^X$ , two states for  $3a_0^X$ , and three states for  $4a_0^X$  and  $5a_0^X$ .

We encounter an increase of the absolute values of exciton  $E_b^X(L)$  and biexciton  $E_b^{XX}(L)$  binding energies with de-

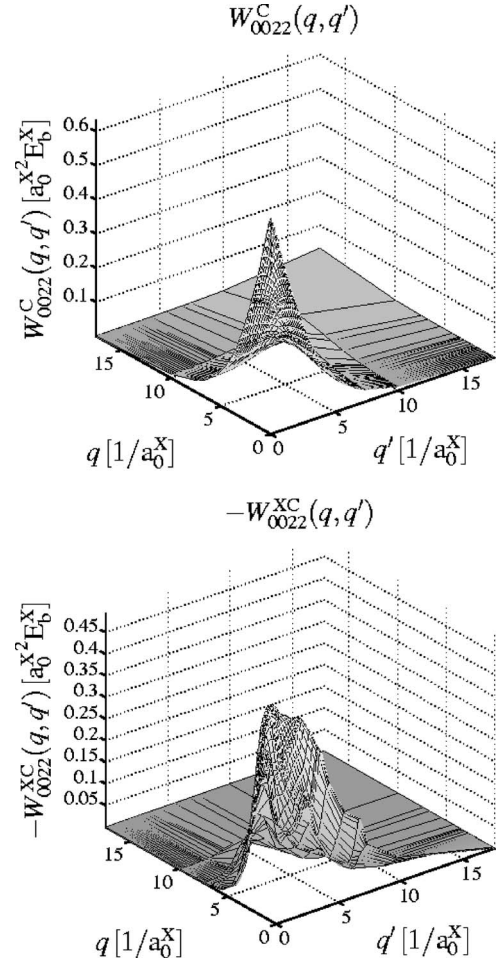


FIG. 4. Examples for off-diagonal Coulomb matrix elements. Direct (top) and exchange (bottom) exciton-exciton interaction.

creasing layer thickness, caused by the quantum confinement of the carriers in one dimension. The biexciton binding energy shows a slightly faster growth than the exciton binding energy due to the larger spatial extension of the biexcitons as

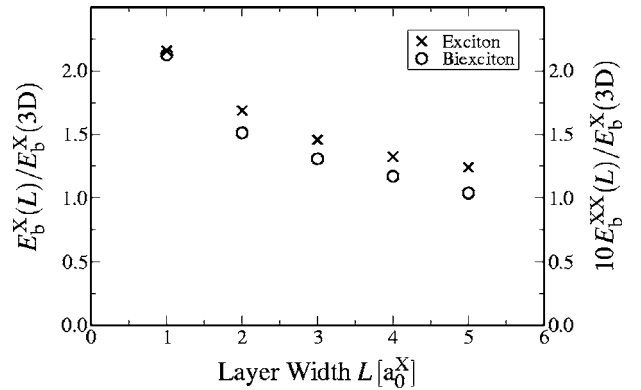


FIG. 5. Dependence of exciton  $E_b^X(L)$  and biexciton  $E_b^{XX}(L)$  binding energy on the layer thickness  $L$ . The exciton binding energy (x) is given with the vertical axis on the left and ten times the biexciton binding energy (o) is given with the vertical axis on the right. Results are normalized to the bulk exciton binding energy  $E_b^X(3D)$ .

already observed before in Refs. 42 and 43 by means of variational methods. The absolute value of the biexciton binding energy might be slightly underestimated in our approach which is caused by the neglect of higher exciton states in the eigenfunction expansion (18). However, we find a confirmation of Hayne's rule:<sup>44</sup> the biexciton binding energy is roughly 10% of the exciton binding energy. In contrast to Refs. 45 and 46 our results show only a slight growth of the exciton-biexciton binding energy ratio  $E_b^X(L)/E_b^{XX}(L)$  for decreasing layer thickness. It turns out that the main contribution to the bound biexciton stems from the exciton ground state; higher exciton states yield only small additional corrections, at least for the considered layer thicknesses. We find higher exciton states becoming more important for the biexciton ground state with increasing layer thickness, which is caused by the decreasing energy level spacing in the exciton spectrum. For  $L=4a_0^X$  the inclusion of two excited excitonic states increases the biexciton binding energy by 9.4% whereas for  $L=5a_0^X$  we encounter an increase of 10.5%.

The presented approach allows a full microscopic description of the biexcitonic correlations and circumvents a simplified evaluation in terms of a one-dimensional tight-binding model as used in previous approaches.<sup>47,48</sup> The discussion of the biexciton binding energy is used here as an indicator for the validity of our eigenfunction expansion. In conclusion, the applied eigenfunction expansion is demonstrated to be a meaningful approximation to incorporate the main physical features of excitonic and biexcitonic states even beyond the quasi-two-dimensional limit of a quantum well.

### B. Nonlinear optics

In this section we present results obtained for the optical transmission spectra of a  $5a_0^X$  GaAs layer with a dipole coupling constant  $d_{eh}/e=5$  Å. A dephasing constant  $\gamma=0.6$  meV for the excitonic polarization and  $2\gamma$  for the biexcitonic correlation function has been included.<sup>49</sup> 120 fs light pulses are applied for the optical excitation which are tuned to the lowest exciton resonance.

The solid line in Fig. 6(a) shows the calculated linear transmission spectrum of the  $5a_0^X$  GaAs layer. The spectral shape of the laser pulse is included as dashed line. The excitation energy is given relative to the bulk band gap energy  $E_{gap}$  and normalized to the corresponding exciton binding energy  $E_b^X$ . Three spectrally well separated polariton modes are observed in the displayed part of the spectrum. They can be attributed to the three lowest exciton states in the confinement geometry and are labeled according to their  $1s$  in-plane symmetry and with consecutive numbers to distinguish their spatial structure in the  $z$  direction.

The diagonalization of the biexcitonic Hamiltonian matrix  $H_{nmn'm'}^{XX\lambda}(\mathbf{q}, \mathbf{q}')$  in the two-exciton product basis yields the biexcitonic spectrum which is depicted in Fig. 6(b) for the electronic singlet ( $\times$ ) and triplet (+) configuration. The discrete structure of the biexcitonic spectrum on the high energy side of the  $1s,1$  polariton resonance, the exciton-exciton scattering continuum, is a consequence of the numerical discretization of the two-exciton relative momentum  $\mathbf{q}$  and of

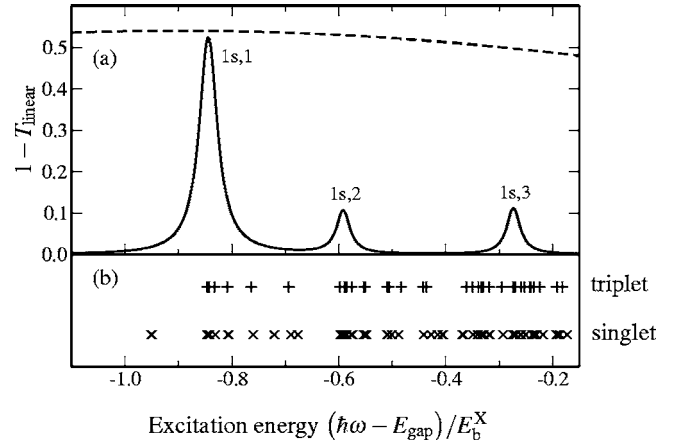


FIG. 6. (a) Calculated linear transmission spectrum (depicted as  $1 - T_{\text{linear}}$ ) for a  $5a_0^X$  GaAs layer (solid line), and spectral shape of the 120 fs laser pulse (dashed line). The polariton resonances are labeled according to the in-plane  $1s$  symmetry of the involved exciton states and with consecutive numbers. (b) Spectral positions of biexciton states for electronic singlet ( $\times$ ) and triplet (+) configuration.

the confinement of electrons and holes in the slab geometry. However, with the finite dephasing constant for the biexcitonic correlations good convergence of the contributions from the biexcitonic continuum to optical spectra is obtained. The bound biexciton state on the low energy side of the  $1s,1$  polariton resonance is found in the electronic singlet subspace in analogy to the Hydrogen molecule problem.

### 1. Single pulse propagation

As a first example we study the nonlinear transmission spectra for a single light pulse. The evaluation is done according to the equations of motion (19) and (20). Restriction of the theory to third order nonlinearities requires the linearization of Eq. (19) to calculate the source terms for the third order response. However, due to the self-consistent coupling of material polarization and light field, also the propagating field contains third order contributions in the field itself which prevents the linearization of Eq. (19). Therefore, with the inclusion of propagation effects a rigorous restriction to third order nonlinearities is no longer possible here. Nevertheless, a consistent description in terms of the derived  $\chi^{(3)}$  theory is obtained by self-consistent evaluation of Eqs. (19) and (20) for sufficiently weak external fields. For a Rabi energy of  $d_{eh}|\mathbf{E}|=0.01E_b^X(3D)$ , used in Fig. 7(b), the nonlinear contributions to the transmitted signal are less than 1% of the linear transmission.

To visualize changes of the transmission itself in Fig. 7(a), an increased Rabi energy of  $d_{eh}|\mathbf{E}|=0.07E_b^X(3D)$  is necessary. For this excitation intensity also higher order nonlinearities beyond the  $\chi^{(3)}$  limit contribute to the nonlinear transmitted signals in Fig. 7(a). The self-consistent evaluation of the equations of motion for the propagating light fields and the material polarization readily includes parts of the higher order nonlinearities, especially the dominant corrections on the  $\chi^{(5)}$  level.

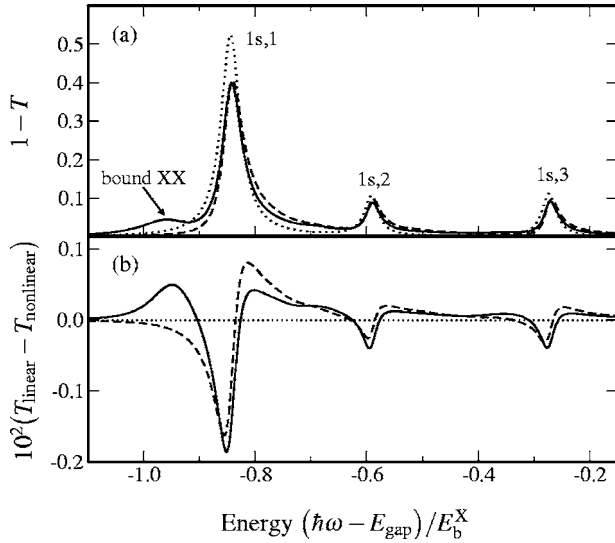


FIG. 7. (a) The dotted line shows the linear transmission spectrum for a  $5a_0^X$  GaAs layer [same as solid line in Fig. 6(a)]. Nonlinear transmission spectra for linear (solid line) and circular (dashed line) light polarization are included for a Rabi energy  $d_{\text{ch}}|\mathbf{E}|=0.07E_b^X$ . (b) Differential single pulse transmission spectra for linear (solid line) and circular (dashed line) light polarization, corresponding to (a) but for a Rabi energy  $d_{\text{ch}}|\mathbf{E}|=0.01E_b^X$ .

The observed bleaching of polariton resonances in Fig. 7 results from Hartree-Fock as well as biexcitonic contributions to the nonlinear optical response. Pauli-blocking and the mean-field contributions to the exciton-exciton Coulomb interaction manifest on the effective two-particle level. Biexcitonic (four-particle) correlations, which are included in the theory presented here, yield additional important contributions. The exciton-exciton Coulomb interaction involves exciton states with nonvanishing in-plane COM momentum in the semiconductor nonlinear optical response. The resulting broad background on the high energy side of the  $1s,1$  resonance is due to excitation of this exciton-exciton scattering continuum.

An advantage of the theoretical approach applied here is the simultaneous inclusion of the bound biexciton state and the exciton-exciton scattering continuum. The latter is essential to reproduce the broad background on the high energy side of the polariton resonances in the nonlinear transmission spectra. For circular light polarization only the biexcitonic continuum states with electronic triplet configuration are excited whereas for linear light polarization both singlet and triplet biexcitonic states contribute to the transmitted signal as visualized in Fig. 8.

A transmission change spectrally below the  $1s,1$  polariton resonance at the spectral position of the bound biexciton (bound XX) state is found for linear light polarization only. Linearly polarized light contains both circularly polarized components which allows the excitation of the bound biexciton state according to its electronic singlet symmetry as depicted in Fig. 8. Excitation of the biexcitonic continuum is possible with either circular or linear light polarization.

## 2. Pump and probe

To provide further insight into the nature of coherent nonlinear polariton saturation, we also studied excitations in a

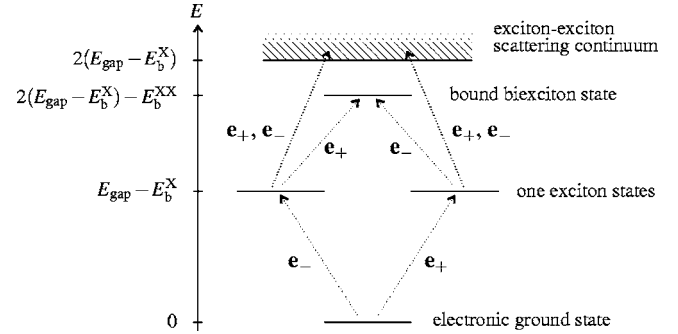


FIG. 8. Schematic illustration of the excitation energies and selection rules for optical excitation of excitons and biexcitons.

pump and probe geometry, where two 120 fs laser pulses (from slightly different directions) without time delay are applied. The selection rules for both pulses are assumed to be those for normal incidence. The probe transmission without pump pulse and the spectral shape of both pulses are displayed in Fig. 6(a). Figure 9(a) shows changes in the probe pulse transmission that are induced by the pump pulse for opposite circular  $\mathbf{e}_+\mathbf{e}_-$  (solid line) and cocircular  $\mathbf{e}_+\mathbf{e}_+$  (dashed-dotted line) polarization of pump and probe pulses. The probe pulse enters the excitonic polarization in linear order only. For the pump pulse a Rabi energy  $d_{\text{ch}}|\mathbf{E}_{\text{pump}}|=0.01E_b^X$  is used. The transmission changes around the

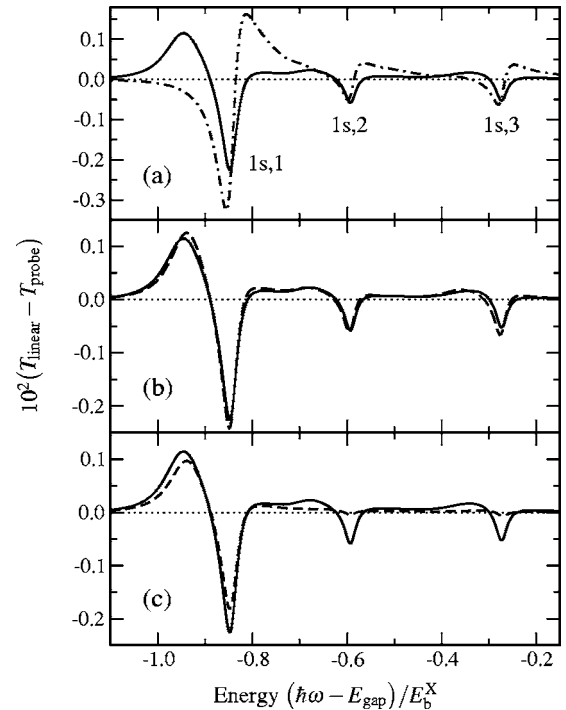


FIG. 9. (a) Differential probe transmission for opposite circular  $\mathbf{e}_+\mathbf{e}_-$  configuration (solid line) and cocircular  $\mathbf{e}_+\mathbf{e}_+$  configuration (dashed-dotted line). (b) Differential probe transmission for  $\mathbf{e}_+\mathbf{e}_-$  configuration including all Coulomb terms [solid line, same as solid line in (a) and (c)], and diagonal Coulomb interaction with respect to the internal exciton quantum numbers in the two-exciton product basis (dashed line). (c) No Coulomb interaction of different excitons (dashed line).

higher ( $1s,2$  and  $1s,3$ ) polariton resonances in Fig. 9(a) are similar to those around the lowest one ( $1s,1$ ) but with a decreased amplitude. In the  $\mathbf{e}_+\mathbf{e}_-$  configuration the excitation of the bound biexciton resonance yields a line shape for the probe transmission changes which corresponds to a redshift of the  $1s,1$  polariton resonance. For the  $\mathbf{e}_+\mathbf{e}_+$  configuration a clear blueshift is observed for the  $1s,1$  polariton resonance. A similar dependence on the light polarization has been reported for the differential probe absorption around the  $1s$  exciton resonance in a QW system.<sup>29</sup>

For opposite-circular  $\mathbf{e}_+\mathbf{e}_-$  polarization, the pump-induced changes in the probe transmission are exclusively determined by biexcitonic correlations;<sup>29</sup> no mean-field effects contribute. On the Hartree-Fock level there would be no coupling of the different transition channels excited with  $\mathbf{e}_+$  and  $\mathbf{e}_-$  light polarization. This configuration is chosen for the analysis of the Coulomb interaction between polaritons in states with different spatial distribution.

As introduced in Sec. III A, we use again the classification of the Coulomb matrix elements (B1) and (B2) by *on-site*, *intersite diagonal*, and *off-diagonal* blocks. Figure 9(b) shows the probe transmission change for a calculation with all Coulomb terms turned on (solid line), and without off-diagonal elements (dashed line). While the qualitative shape of transmission changes is only slightly influenced by the off-diagonal terms, they lead to an increase of the biexciton binding energy by about 10%. Off-diagonal contributions become more important for increasing layer thickness where the energetical spacing of excitonic states decreases and the excited states play a more important role, even for the biexciton ground state.

The dashed line in Fig. 9(c) shows the result where Coulomb interaction that couples different exciton states in the two-exciton product basis of Eq. (18) is completely switched off. We encounter only a slight change of the transmission changes around the lowest polariton resonance ( $1s,1$ ) whereas for higher peaks ( $1s,2$  and  $1s,3$ ) the influence of the pump pulse almost vanishes. The neglect of both off-diagonal terms and inter-site diagonal elements prevents the formation of biexciton states by interaction of excitons in different states.

Thinking in a simplified exciton picture these results lead to the following conclusion: The transmission changes around the ( $1s,1$ ) resonance are dominated by contributions from ( $1s,1$ )( $1s,1$ ) biexcitons, namely biexcitons built up from two ( $1s,1$ ) excitons. However, the transmission changes around the higher resonances are dominated by contributions from ( $1s,1$ )( $1s,2$  or  $3$ ) biexcitons. We only find a small contribution from biexcitons solely built up of excited excitons because of the weak oscillator strength of the connected exciton states. As a result, Coulomb interaction of excitons in states with different spatial distribution (corresponding to different polariton resonances) turns out to be the main source for transmission changes of higher polariton states.

### 3. Four-wave mixing

The evaluation of four-wave mixing signals in this section is based on the equations of motion for the third order ma-

terial polarization, Eqs. (17) and (18). Two 120 fs laser pulses are applied (from slightly different directions  $\mathbf{k}_1$  and  $\mathbf{k}_2$ ) with the spectral shape which is depicted in Fig. 6(a). Again the dipole selection rules are assumed to be those for normal incidence. The diffracted four-wave mixing signal is observed in the  $2\mathbf{k}_2-\mathbf{k}_1$  direction and is exclusively sensitive to third order nonlinearities in the optically induced material polarization. It is not superimposed by a linear background transmission of one of the incoming pulses. For the laser pulse in  $\mathbf{k}_2$  direction a Rabi energy of  $d_{\text{ch}}|\mathbf{E}|=0.01E_b^X$  is used to ensure a consistent evaluation within our  $\chi^{(3)}$  theory. Results are presented for the GaAs model system with a layer thickness of  $5a_0^X$  as in the previous sections. To give a comparison to a quasi-two-dimensional quantum-well system, results are also shown for a layer thickness of  $1a_0^X$ . Four-wave mixing signals are analyzed as a function of the delay time  $t_{\text{del}}$  between the two incoming light pulses for different polarization states of the fields. The detection is assumed to be insensitive to the polarization state of the diffracted signal in  $2\mathbf{k}_2-\mathbf{k}_1$  direction.

The calculated spectrally resolved four-wave mixing signal is shown in Fig. 10 for cocircular  $\mathbf{e}_+\mathbf{e}_+$  polarization of the two incident light pulses, in Fig. 11 for colinear  $\mathbf{e}_x\mathbf{e}_x$  polarization, and in Fig. 12 for cross-linear  $\mathbf{e}_x\mathbf{e}_y$  polarization, respectively. The magnitude of the four-wave mixing intensity is visualized by the color coding on a logarithmic scale. In the upper part of each figure, the result for  $5a_0^X$  layer thickness is depicted and in the lower part the corresponding result for the quantum-well system with  $1a_0^X$  layer thickness is shown.

For the  $5a_0^X$  system, both pulses are centered at an excitation energy of  $-0.6$  in excitonic units as given at the horizontal axis of Fig. 6. The energies of the excitonic resonances for the quantum well with  $1a_0^X$  thickness are shifted to higher values due to the confinement of the carrier motion in the  $z$  direction. Therefore, for this system, the pulses are centered on the spectral position of the exciton resonance at  $7.71$  in excitonic units.

For the  $5a_0^X$  sample and all three configurations, a four-wave mixing signal is detected at the spectral position of the three polariton resonances which are visible in the linear transmission spectrum of Fig. 6(a). Qualitatively, around the spectral position of the lowest polariton resonance a similar polarization dependence of the four-wave mixing signal is observed as it is found for the  $1a_0^X$  quantum-well system: (i) For the  $\mathbf{e}_+\mathbf{e}_+$  configuration in Fig. 10 no resonant contribution to the signal is detected at the spectral position of the bound biexciton state, according to its electronic singlet configuration as already discussed in the previous sections. A fast decay of the signal for negative delay times  $t_{\text{del}} < 0$  is found. (ii) For the  $\mathbf{e}_x\mathbf{e}_x$  configuration in Fig. 11 the signal is dominated by contributions at the spectral positions of the polariton resonances while the signal at the spectral position of the bound biexciton resonance is weak in this configuration. (iii) For the  $\mathbf{e}_x\mathbf{e}_y$  configuration in Fig. 12 a resonant contribution to the four-wave mixing signal is visible at the spectral position of the bound biexciton resonance spectrally

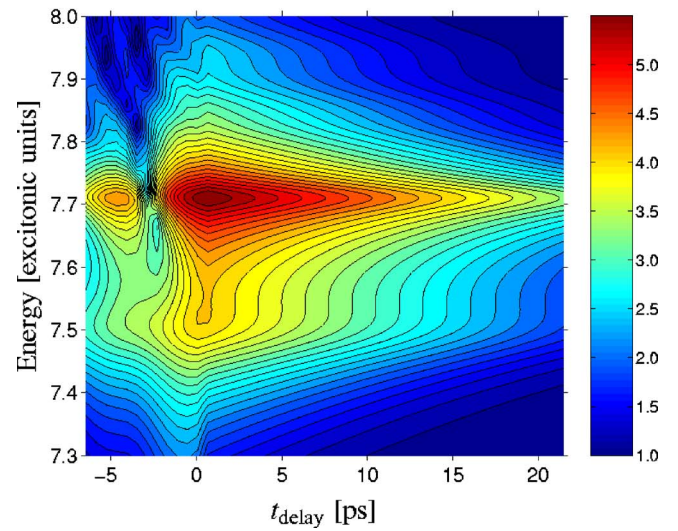
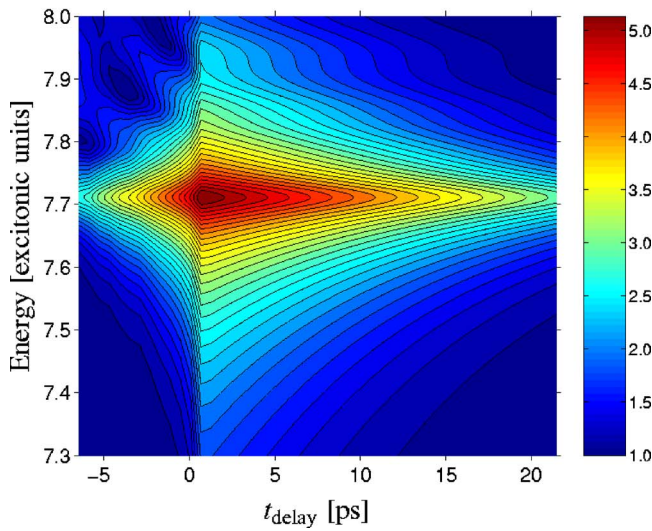
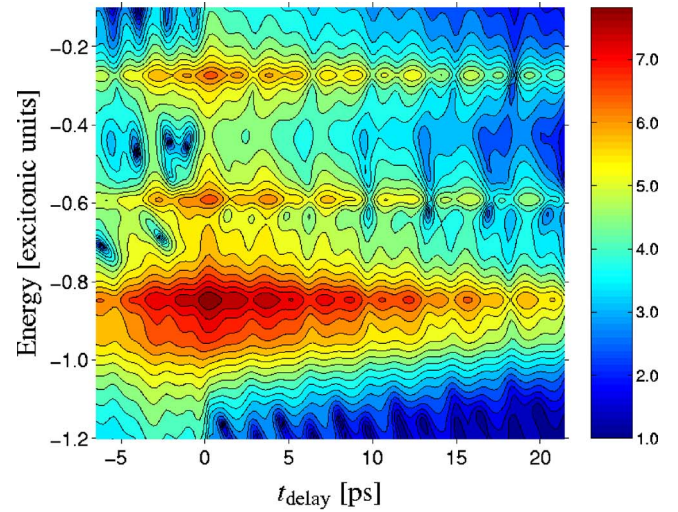
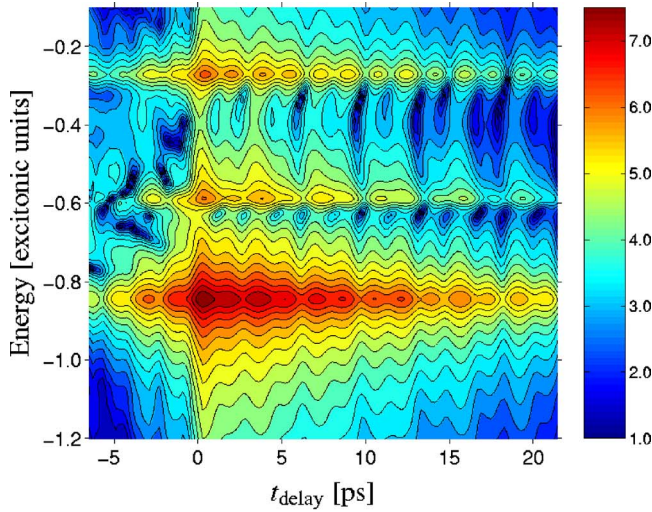


FIG. 10. (Color online) Top: Contour plot of the spectrally resolved four-wave mixing intensity in cocircular  $\mathbf{e}_+\mathbf{e}_+$  configuration as a function of the delay time  $t_{\text{delay}}$  between the two incoming light pulses for a GaAs layer with thickness of  $5a_0^X$ . The color coding represents the four-wave mixing intensity in arbitrary units on a logarithmic scale according to the color bar. The energy scale on the vertical axis is chosen in excitonic units according to the horizontal axis in Fig. 6. Bottom: Same as upper part but for a quantum well with layer thickness of  $1a_0^X$ .

FIG. 11. (Color online) Same as Fig. 10 but for colinear  $\mathbf{e}_x\mathbf{e}_x$  polarization of the two incoming light pulses.

below the lowest polariton resonance. This feature is much more pronounced for the  $1a_0^X$  system because of the larger biexciton binding energy and the smaller spectral window which is displayed in the figures. However, comparing Figs. 11 and 12, also for the  $5a_0^X$  system a qualitative difference in the four-wave mixing signals spectrally below the lowest polariton resonance is visible. It can be attributed to the excitation of the bound biexciton resonance. A similar polarization dependence of four-wave mixing signals has experimentally and theoretically been observed for a ZnSe quantum-well system in Refs. 50 and 51.

For the system with  $5a_0^X$  layer thickness we find that the

detected signal at the spectral position of each polariton resonance is strongly influenced by the excitation of the other resonances. In the displayed spectral range the signal is periodically modulated in the delay time  $t_{\text{delay}}$ . These oscillations are absent for the quantum-well system since only a single excitonic resonance contributes to the four-wave mixing signal. The periods of the oscillations are determined by the energy separation of the different polariton resonances. Two main contributions to these oscillations can be attributed to the larger energy difference between first and third polariton resonance and to the smaller energy difference between first and second or second and third resonance, respectively. Oscillations have also been observed in QW systems due to the interference of contributions from exciton and biexciton at higher excitation conditions.<sup>33,51</sup> In our case, the signal at higher polariton resonances is influenced by the scattering continuum of the lower resonances. It should be noted that an interpretation in terms of independent polariton resonances is not valid beyond the quantum-well limit since a

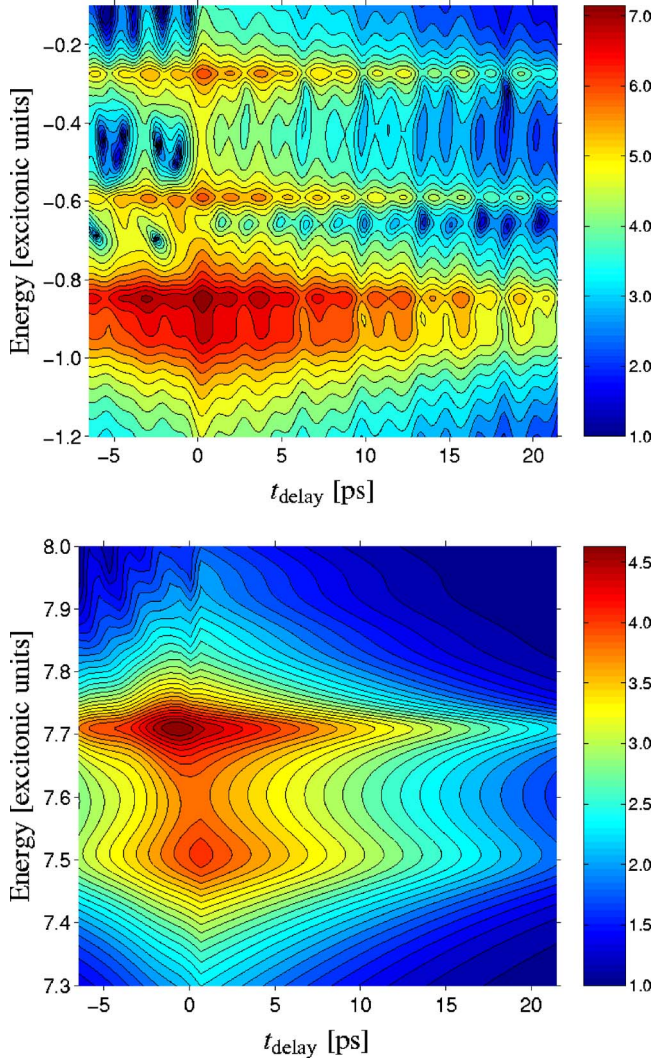


FIG. 12. (Color online) Same as Fig. 10 but for cross-linear  $\mathbf{e}_x\mathbf{e}_y$  polarization of the two incoming light pulses.

strong interaction of the contributions from different polariton resonances over the whole spectral range is observed.

#### IV. CONCLUSION

A theory for the nonlinear polariton dynamics in semiconductor heterostructures has been presented which consistently includes (i) propagation effects with microscopic boundary conditions for the induced material polarization as well as for the optical fields and (ii) excitonic and biexcitonic coherent nonlinearities previously studied only in QWs or one-dimensional model systems. The numerically extremely demanding theory has been evaluated by an efficient expansion of excitonic polarization and biexcitonic correlation function in terms of excitonic eigenstates of the slab geometry. As an important indicator for a proper description of biexcitonic correlations within this approach, the biexcitonic spectral properties have been investigated in detail. Espe-

cially, the dependence of the biexciton binding energy on the layer thickness has been discussed. The influence of light-polarization dependent excitonic and biexcitonic nonlinearities has been demonstrated and analyzed in detail for the propagation of a single light pulse as well as in typical pump and probe and four-wave mixing geometries. For the heterostructures investigated in this work with layer thicknesses beyond the quasi-two-dimensional quantum-well limit, the Coulomb interaction of polariton states with different spatial distribution has been shown to strongly influence nonlinear optical transmission spectra.

#### ACKNOWLEDGMENTS

We acknowledge a grant for CPU time from the John von Neumann Institute for Computing at the Forschungszentrum Jülich.

#### APPENDIX A: DYNAMICS-CONTROLLED TRUNCATION

In this section we provide the relations for the dynamics-controlled truncation of density matrix elements in the coherent  $\chi^{(3)}$  limit which are used to deduce the equations of motion (14) and (16) along the lines described in Ref. 39.

The occupation functions up to third order in the optical field in the coherent limit are

$$\langle \psi_{\mathbf{k}}^{e'\dagger}(z_h) \psi_{\mathbf{k}}^e(z_e) \rangle \approx \sum_h \int dz p_{(\mathbf{k}, z_h, z)}^{*e'h} p_{(\mathbf{k}, z_e, z)}^{eh} \quad (\text{A1})$$

for the conduction band and

$$\langle \psi_{\mathbf{k}}^{h'\dagger}(z_e) \psi_{\mathbf{k}}^h(z_h) \rangle \approx \sum_e \int dz p_{(\mathbf{k}, z_e, z)}^{*eh'} p_{(\mathbf{k}, z, z_h)}^{eh} \quad (\text{A2})$$

for the valence band. The four-point functions, which appear in the equation of motion for the excitonic polarization up to third order in the external fields, are the electron-assisted transition amplitude

$$\begin{aligned} & \langle \psi_{\mathbf{k}_1}^{e'\dagger}(z) \psi_{\mathbf{k}_2}^{e'}(z) \psi_{\mathbf{k}_3}^h(z_h) \psi_{\mathbf{k}_4}^e(z_e) \rangle \\ & \approx \sum_{h'} \int dz' p_{(\mathbf{k}_1, z, z')}^{*e'h'} \langle \psi_{\mathbf{k}_1}^{h'}(z') \psi_{\mathbf{k}_2}^{e'}(z) \psi_{\mathbf{k}_3}^h(z_h) \psi_{\mathbf{k}_4}^e(z_e) \rangle, \end{aligned} \quad (\text{A3})$$

and the hole-assisted transition amplitude

$$\begin{aligned} & \langle \psi_{\mathbf{k}_1}^{h'\dagger}(z) \psi_{\mathbf{k}_2}^{h'}(z) \psi_{\mathbf{k}_3}^h(z_h) \psi_{\mathbf{k}_4}^e(z_e) \rangle \\ & \approx \sum_{e'} \int dz' p_{(\mathbf{k}_1, z', z)}^{*e'h'} \langle \psi_{\mathbf{k}_2}^{h'}(z) \psi_{\mathbf{k}_1}^{e'}(z') \psi_{\mathbf{k}_3}^h(z_h) \psi_{\mathbf{k}_4}^e(z_e) \rangle, \end{aligned} \quad (\text{A4})$$

which are given here in the coherent limit.

#### APPENDIX B: MATRIX ELEMENTS

With  $\mathbf{q}^+ = \mathbf{q} + \mathbf{q}'$  and  $\mathbf{q}^- = \mathbf{q} - \mathbf{q}'$  the Coulomb matrix elements in the two-exciton product basis are given by

$$\begin{aligned}
W_{nmn'm'}^C(\mathbf{q}, \mathbf{q}') &= \sum_{\mathbf{k}\mathbf{k}'} \int dz_e dz_h dz_{e'} dz_{h'} \phi_n^*(\mathbf{k}, z_e, z_h) \phi_m^*(\mathbf{k}', z_{e'}, z_{h'}) [V_{\mathbf{q}^-}^{z_h' z_h} \phi_{n'}(\mathbf{k} + \beta \mathbf{q}^-, z_e, z_h) \phi_{m'}(\mathbf{k}' - \beta \mathbf{q}^-, z_{e'}, z_{h'}) \\
&\quad + V_{\mathbf{q}^-}^{z_e' z_e} \phi_{n'}(\mathbf{k} - \alpha \mathbf{q}^-, z_e, z_h) \phi_{m'}(\mathbf{k}' + \alpha \mathbf{q}^-, z_{e'}, z_{h'}) - V_{\mathbf{q}^-}^{z_e' z_h} \phi_{n'}(\mathbf{k} + \beta \mathbf{q}^-, z_e, z_h) \phi_{m'}(\mathbf{k}' + \alpha \mathbf{q}^-, z_{e'}, z_{h'}) \\
&\quad - V_{\mathbf{q}^-}^{z_h' z_e} \phi_{n'}(\mathbf{k} - \alpha \mathbf{q}^-, z_e, z_h) \phi_{m'}(\mathbf{k}' - \beta \mathbf{q}^-, z_{e'}, z_{h'})], \tag{B1}
\end{aligned}$$

for the direct part, and

$$\begin{aligned}
W_{nmn'm'}^{XC}(\mathbf{q}, \mathbf{q}') &= \sum_{\mathbf{k}\mathbf{k}'} \int dz_e dz_h dz_{e'} dz_{h'} \phi_n^*(\mathbf{k} + \alpha \mathbf{q}^-, z_e, z_h) \phi_m^*(\mathbf{k}' + \beta \mathbf{q}^+, z_{e'}, z_{h'}) \{ \phi_{n'}(\mathbf{k}', z_{e'}, z_{h'}) [V_{\mathbf{k}-\mathbf{k}'}^{z_e z_h} \phi_{m'}(\mathbf{k}' + \alpha \mathbf{q}^- + \beta \mathbf{q}^+, z_e, z_{h'}) \\
&\quad - V_{\mathbf{k}-\mathbf{k}'}^{z_h' z_h} \phi_{m'}(\mathbf{k} + \alpha \mathbf{q}^- + \beta \mathbf{q}^+, z_e, z_{h'})] + \phi_{n'}(\mathbf{k}, z_{e'}, z_{h'}) [V_{\mathbf{k}-\mathbf{k}'}^{z_h' z_e'} \phi_{m'}(\mathbf{k} + \alpha \mathbf{q}^- + \beta \mathbf{q}^+, z_e, z_{h'}) \\
&\quad - V_{\mathbf{k}-\mathbf{k}'}^{z_e z_e'} \phi_{m'}(\mathbf{k}' + \alpha \mathbf{q}^- + \beta \mathbf{q}^+, z_e, z_{h'})] \} \tag{B2}
\end{aligned}$$

for the two-exciton exchange interaction. The biexcitonic Hamiltonian matrix in this basis has the form

$$\begin{aligned}
H_{nmn'm'}^{XX\lambda}(\mathbf{q}, \mathbf{q}') &= [\varepsilon_n(q) + \varepsilon_m(q)] \delta_{nn'} \delta_{mm'} \delta_{\mathbf{q}\mathbf{q}'} \\
&\quad + \sum_{rs\mathbf{k}} (1 - \lambda S)_{nmrs}^{-1}(\mathbf{q}, \mathbf{k}) W_{rsn'm'}^{XX\lambda}(\mathbf{k}, \mathbf{q}'), \tag{B3}
\end{aligned}$$

using

$$W_{nmn'm'}^{XX\lambda}(\mathbf{q}, \mathbf{q}') = W_{nmn'm'}^C(\mathbf{q}, \mathbf{q}') + \lambda \cdot W_{nmn'm'}^{XC}(\mathbf{q}, \mathbf{q}') \tag{B4}$$

and the exciton overlap matrix elements

$$\begin{aligned}
S_{nmn'm'}(\mathbf{q}, \mathbf{q}') &= \sum_{\mathbf{k}} \int dz_e dz_h dz_{e'} dz_{h'} \\
&\quad \times \phi_n^*(\mathbf{k} + \alpha \mathbf{q}, z_e, z_h) \phi_m^*(\mathbf{k} + \mathbf{q}' + \beta \mathbf{q}, z_{e'}, z_{h'}) \\
&\quad \times \phi_{n'}(\mathbf{k} + \alpha \mathbf{q}', z_{e'}, z_{h'}) \\
&\quad \times \phi_{m'}(\mathbf{k} + \mathbf{q} + \beta \mathbf{q}', z_e, z_{h'}). \tag{B5}
\end{aligned}$$

The Hartree-Fock Coulomb matrix elements are obtained from the  $\mathbf{q} \rightarrow 0, \mathbf{q}' \rightarrow 0$  limit of the two-exciton exchange matrix elements (B2):

$$V_{mm'n'm'}^{HF} = W_{n'nmn'}^{XC*}(0, 0). \tag{B6}$$

The Hartree-Fock matrix elements for the phase-space filling corrections (Pauli blocking) to the Rabi energy are

$$R_{nmn'n}^1(z) = \sum_{\mathbf{k}} \int dz' dz'' \phi_m^*(\mathbf{k}, z, z'') \phi_{m'}(\mathbf{k}, z', z) \phi_n(\mathbf{k}, z', z'') \tag{B7}$$

and

$$R_{nmn'n}^2(z) = \sum_{\mathbf{k}} \int dz' dz'' \phi_m^*(\mathbf{k}, z'', z) \phi_{m'}(\mathbf{k}, z, z') \phi_n(\mathbf{k}, z'', z'). \tag{B8}$$

Expansion of the real space dependence of the exact exciton eigenfunctions  $\phi_m(\mathbf{k}, z_e, z_h)$  in terms of products of one-particle eigenstates in the  $z$  direction

$$\phi_m(\mathbf{k}, z_e, z_h) = \sum_{ij} a_{ij}^m(\mathbf{k}) \chi_i(z_e) \varphi_j(z_h), \tag{B9}$$

yields a multisubband version of the matrix elements (B1) to (B8). In the one-subband limit and for identical one-particle envelope wave functions  $\chi_i(z_e)$  and  $\varphi_j(z_h)$  for electrons and holes, respectively, the theory for the two-dimensional or one-subband quantum well<sup>36</sup> is reproduced with  $a_{00}^m(\mathbf{k})$  being the two-dimensional in-plane exciton wave function.

### APPENDIX C: NUMERICS

The evaluation of the Coulomb matrix elements in the two-exciton product basis turns out to be numerically very demanding. Especially parts of the exchange interaction matrix element (B2) with its fourfold real space integral cannot be factorized. Of particular importance is a proper treatment of the Coulomb singularity in  $W_{nmn'm'}^C(\mathbf{q}, \mathbf{q}')$  and  $W_{nmn'm'}^{XC}(\mathbf{q}, \mathbf{q}')$  which has been removed numerically. The independent calculations of the matrix elements can be performed efficiently on parallel computers. Once evaluated, the matrix elements can be stored for each given set of material parameters. Using this input data the solution of the equations of motion can be performed on a desktop computer, using a fourth order Runge-Kutta algorithm for the material equations (19) and (20) and Hartree's method for the discretization of Maxwell's equations (12) and (13). The solutions are obtained in the time domain in the rotating wave picture to eliminate the large band gap energy in the material equations. Details concerning Hartree's method are given in

Ref. 52 and their application to the one-dimensional Maxwell equations is briefly summarized in Ref. 16.

For a proper evaluation of the matrix elements the numerical discretization scheme of real space coordinates and in-plane momenta has to be chosen very carefully. We use Gaussian quadrature points for the calculation of  $k$ -space integrals, which provide much better numerical convergence with a small number of quadrature points, compared to an equidistantly chosen grid. For the exciton wave functions we

typically used a real space step size of  $\approx 0.1a_0^X$  and 70 Gaussian  $k$  quadrature points accumulated below  $k=20/a_0^X$ . Biexciton grid points were chosen to 16 angle points, 32 Gaussian  $q$  and  $k$  quadrature points and 24 equidistant points for real space integrals. Contributions from in plane momenta  $\mathbf{k}$  with  $k > 20/a_0^X$  are neglected in a very good approximation because wave functions and Coulomb matrix elements rapidly decay for large momenta, as can be seen in Figs. 2–4.

- <sup>1</sup>D. Fröhlich, A. Kulik, B. Uebbing, A. Mysyrowicz, V. Langer, H. Stolz, and W. von der Osten, *Phys. Rev. Lett.* **67**, 2343 (1991).
- <sup>2</sup>A. Tredicucci, Y. Chen, F. Bassani, J. Massies, C. Deparis, and G. Neu, *Phys. Rev. B* **47**, 10348 (1993).
- <sup>3</sup>S. Lankes, M. Meier, T. Reisinger, and W. Gebhardt, *J. Appl. Phys.* **80**, 4049 (1996).
- <sup>4</sup>J. Tignon, T. Hasche, D. S. Chemla, H. C. Schneider, F. Jahnke, and S. W. Koch, *Phys. Rev. Lett.* **84**, 3382 (2000).
- <sup>5</sup>S. Schumacher, G. Czycholl, F. Jahnke, I. Kudyk, H. I. Rückmann, J. Gutowski, A. Gust, G. Alexe, and D. Hommel, *Phys. Rev. B* **70**, 235340 (2004).
- <sup>6</sup>U. Neukirch and K. Wundke, *Phys. Rev. B* **55**, 15408 (1997).
- <sup>7</sup>S. Schumacher, G. Czycholl, F. Jahnke, I. Kudyk, L. Wischmeier, I. Rückmann, T. Voss, J. Gutowski, A. Gust, and D. Hommel, *Phys. Rev. B* **72**, 081308(R) (2005).
- <sup>8</sup>H. Haug and S. W. Koch, *Quantum Theory of the Optical and Electronic Properties of Semiconductors*, 3rd ed. (World Scientific, Singapore, 1995).
- <sup>9</sup>A. D'Andrea and R. Del Sole, *Phys. Rev. B* **25**, 3714 (1982).
- <sup>10</sup>A. Stahl and I. Balslev, *Electrodynamics of the Semiconductor Band Edge*, Springer Tracts in Modern Physics, Vol. 10 (Springer, New York, 1987).
- <sup>11</sup>I. Balslev, R. Zimmermann, and A. Stahl, *Phys. Rev. B* **40**, 4095 (1989).
- <sup>12</sup>A. D'Andrea and R. Del Sole, *Phys. Rev. B* **41**, 1413 (1990).
- <sup>13</sup>S. I. Pekar, *Sov. Phys. JETP* **6**, 785 (1958).
- <sup>14</sup>C. S. Ting, M. J. Frankel, and J. L. Birman, *Solid State Commun.* **17**, 1285 (1975).
- <sup>15</sup>E. F. Venger and V. N. Piskovoi, *Phys. Rev. B* **70**, 115107 (2004).
- <sup>16</sup>H. C. Schneider, F. Jahnke, S. W. Koch, J. Tignon, T. Hasche, and D. S. Chemla, *Phys. Rev. B* **63**, 045202 (2001).
- <sup>17</sup>E. A. Muljarov and R. Zimmermann, *Phys. Rev. B* **66**, 235319 (2002).
- <sup>18</sup>S. Schumacher, G. Czycholl, and F. Jahnke, *Phys. Status Solidi B* **234**, 172 (2002).
- <sup>19</sup>G. Khitrova, H. M. Gibbs, F. Jahnke, M. Kira, and S. W. Koch, *Rev. Mod. Phys.* **71**, 1591 (1999).
- <sup>20</sup>T. Meier, C. Sieh, S. W. Koch, Y.-S. Lee, T. B. Norris, F. Jahnke, G. Khitrova, and H. M. Gibbs, in *Nonlinear Optical Properties of Semiconductor Quantum Wells Inside Microcavities*, Optical Microcavities, edited by K. Vahala (World Scientific, Singapore, 2004), Chap. 6, pp. 239–317.
- <sup>21</sup>H. Giessen, A. Knorr, S. Haas, S. W. Koch, S. Linden, J. Kuhl, M. Hetterich, M. Grün, and C. Klingshirm, *Phys. Rev. Lett.* **81**, 4260 (1998).
- <sup>22</sup>J. Förstner, A. Knorr, and S. W. Koch, *Phys. Rev. Lett.* **86**, 476 (2001).
- <sup>23</sup>A. Schulze, A. Knorr, and S. W. Koch, *Phys. Rev. B* **51**, 10601 (1995).
- <sup>24</sup>J. S. Nägerl, B. Stabenau, G. Böhne, S. Dreher, R. G. Ulbrich, G. Manzke, and K. Henneberger, *Phys. Rev. B* **63**, 235202 (2001).
- <sup>25</sup>V. M. Axt and A. Stahl, *Z. Phys. B: Condens. Matter* **93**, 195 (1994).
- <sup>26</sup>V. M. Axt and A. Stahl, *Z. Phys. B: Condens. Matter* **93**, 205 (1994).
- <sup>27</sup>M. Lindberg, Y. Z. Hu, R. Binder, and S. W. Koch, *Phys. Rev. B* **50**, 18060 (1994).
- <sup>28</sup>V. M. Axt, A. Stahl, E. J. Mayer, P. Haring Bolivar, S. Nüsse, K. Ploog, and K. Köhler, *Phys. Status Solidi B* **188**, 447 (1995).
- <sup>29</sup>C. Sieh, T. Meier, F. Jahnke, A. Knorr, S. W. Koch, P. Brick, M. Hübner, C. Ell, J. Prineas, G. Khitrova, and H. M. Gibbs, *Phys. Rev. Lett.* **82**, 3112 (1999).
- <sup>30</sup>N. H. Kwong, R. Takayama, I. Romyantsev, M. Kuwata-Gonokami, and R. Binder, *Phys. Rev. B* **64**, 045316 (2001).
- <sup>31</sup>N. H. Kwong, R. Takayama, I. Romyantsev, M. Kuwata-Gonokami, and R. Binder, *Phys. Rev. Lett.* **87**, 027402 (2001).
- <sup>32</sup>M. E. Donovan, A. Schülzgen, J. Lee, P.-A. Blanche, N. Peyghambarian, G. Khitrova, H. M. Gibbs, I. Romyantsev, N. H. Kwong, R. Takayama, Z. S. Yang, and R. Binder, *Phys. Rev. Lett.* **87**, 237402 (2001).
- <sup>33</sup>M. Buck, L. Wischmeier, S. Schumacher, G. Czycholl, F. Jahnke, T. Voss, I. Rückmann, and J. Gutowski, *Eur. Phys. J. B* **42**, 175 (2004).
- <sup>34</sup>T. Meier and S. W. Koch, *Phys. Rev. B* **59**, 13202 (1999).
- <sup>35</sup>H. G. Breunig, T. Voss, I. Rückmann, J. Gutowski, V. M. Axt, and T. Kuhn, *J. Opt. Soc. Am. B* **20**, 1769 (2003).
- <sup>36</sup>R. Takayama, N. H. Kwong, I. Romyantsev, M. Kuwata-Gonokami, and R. Binder, *Eur. Phys. J. B* **25**, 445 (2002).
- <sup>37</sup>W. Schäfer, R. Lövenich, N. A. Fromer, and D. S. Chemla, *Phys. Rev. Lett.* **86**, 344 (2001).
- <sup>38</sup>The Coulomb matrix elements  $V_{\mathbf{k}-\mathbf{k}'}^{zz'}$  with  $|\mathbf{k}-\mathbf{k}'| = \sqrt{k^2+k'^2-2kk'\cos(\phi_k-\phi_{k'})}$  contain the angle  $\phi_k-\phi_{k'}$  which is enclosed by  $\mathbf{k}$  and  $\mathbf{k}'$ .
- <sup>39</sup>W. Schäfer and M. Wegener, *Semiconductor Optics and Transport Phenomena* (Springer, Berlin, 2002).
- <sup>40</sup>The time dependence of the excitonic and biexcitonic expansion coefficients will not be made explicit in the following.
- <sup>41</sup>I. Romyantsev, N. H. Kwong, R. Binder, E. J. Gansen, and A. L. Smirl, *Phys. Rev. B* **69**, 235329 (2004).
- <sup>42</sup>R. C. Miller, D. A. Kleinman, A. C. Gossard, and O. Munteanu, *Phys. Rev. B* **25**, 6545 (1982).
- <sup>43</sup>D. A. Kleinman, *Phys. Rev. B* **28**, 871 (1983).

- <sup>44</sup>J. R. Haynes, Phys. Rev. Lett. **4**, 361 (1960).
- <sup>45</sup>J. Zhang, T. Pang, and C. Chen, Phys. Lett. A **206**, 101 (1995).
- <sup>46</sup>I. K. Oh and J. Singh, Phys. Rev. B **60**, 2528 (1999).
- <sup>47</sup>J. Förstner, A. Knorr, S. Kuckenburg, T. Meier, S. W. Koch, H. Giessen, S. Linden, and J. Kuhl, Phys. Status Solidi B **221**, 253 (2000).
- <sup>48</sup>N. C. Nielsen, S. Linden, J. Kuhl, J. Förstner, A. Knorr, S. W. Koch, and H. Giessen, Phys. Rev. B **64**, 245202 (2001).
- <sup>49</sup>The dephasing constant for the biexcitonic correlations in our model is two times the dephasing constant of the corresponding excitonic polarization. This assumption complies with the intuitive picture that each biexciton is a buildup of two single excitons being both subject to dephasing processes.
- <sup>50</sup>J. Gutowski, H. G. Breunig, and T. Voss, in *Dynamics of Excitons and Exciton Complexes in Wide-Gap Semiconductors*, Springer Series in Solid State Sciences, Vol. 146 Optics of Semiconductors and Their Heterostructures, edited by H. Kalt and M. Hetterich (Springer, Berlin, 2004).
- <sup>51</sup>W. Langbein, T. Meier, S. W. Koch, and J. M. Hvam, J. Opt. Soc. Am. B **18**, 1318 (2001).
- <sup>52</sup>W. F. Ames, *Numerical Methods for Partial Differential Equations*, Computer Science and Scientific Computing, 3rd ed. (Academic Press, San Diego, 1992).